A practical lithium-ion battery model for state of energy and voltage responses prediction incorporating temperature and ageing effects

Kaiyuan Li, Feng Wei, *Member, IEEE*, King Jet Tseng, *Senior Member, IEEE,* and Boon-Hee Soong*, Senior Member, IEEE*

***Abstract*—The state of energy (SOE) is a key indicator for the energy optimization and management of Li-ion battery-based energy storage systems in the smart grid applications. To improve the SOE estimation accuracy, a Li-ion battery model is presented in this study against dynamic loads and battery ageing effects. Firstly, an electrical battery model is combined with an analytical model in order to take advantages of both models for accurate prediction of battery terminal voltage characteristics, SOE and remnant runtime. Secondly, a novel method to separate the fast and slow dynamics of the electrical battery model is developed, and its superior performance is presented. Thirdly, the effects of the battery initial SOC, load current rate and direction, operating temperature and ageing level are systematically scrutinized and involved into the proposed model for robust SOE and terminal voltage prediction. Commercial Li-ion batteries are then tested under dynamic loads and at an arbitrary battery ageing level to validate the effectiveness and robustness of the proposed model. The laboratory-scale experimental test results show superb accuracy and reliability of the proposed battery model for estimating battery SOE and terminal voltage under dynamic loads and battery ageing conditions.**

***Index Terms*—Battery ageing, dynamic loads, electrical battery model, Li-ion battery, State of energy (SOE), terminal voltage characteristic, temperature effects.**

Manuscript received April 10, 2017; revised July 13, 2017; accepted October 13, 2017. This work was supported by the Republic of Singapore's National Research Foundation under its Campus for Research Excellence and Technological Enterprise (CREATE) program through a grant to the Berkeley Education Alliance for Research in Singapore (BEARS) for the Singapore-Berkeley Building Efficiency and Sustainability in the Tropics (SinBerBEST) Program. BEARS has been established by the University of California, Berkeley, as a center for intellectual excellence in research and education in Singapore.

K. Li and B. H. Soong are with the School of Electrical and Electronic Engineering, Nanyang Technological University, Singapore 639798 (e-mail: kli1@e.ntu.edu.sg; ebhsoong@ntu.edu.sg).

F. Wei is with the Berkeley Education Alliance for Research in Singapore, Singapore, 138602 (e-mail: weif0004@ntu.edu.sg).

K.J. Tseng is with the Singapore Institute of Technology, Singapore, 138683 (e-mail: kingjet.tseng@singaporetech.edu.sg).

I. Introduction

SINCE this decade, in order to successfully address the smart grid applications, energy storage systems (ESSs) have been studied extensively. ESS is now playing a pivotal role in propelling the exploitation of renewable energy sources into the traditional energy market and helping to provide stable and reliable power supply in smart grids. Among all the energy storage techniques, Li-ion based rechargeable batteries are deemed to be the most promising solution, due to their outperformed performance such as high gravimetric and volumetric energy density, great cycle life, enhanced safety and low self-discharge rate [1-3].

During battery operations, an indispensable component is the battery management system (BMS), which is responsible for the efficient, reliable, and durable battery operations. Nowadays, modern BMSs rely on battery models to track the key indexes of each cell and further the whole battery system, thusly the exploited models are required to be competent to predict the battery behaviors accurately. Our research is based on a self-operated island smart grid where Li-ion batteries are employed as ESSs, and we are aiming to predict the online state of health (SOH), state of charge (SOC), state of energy (SOE), runtime, and terminal voltage responses of the batteries under varying and unpredictable load conditions with high accuracy and robustness. Amongst these indexes, SOE has been replacing SOC these years to represent the residual energy of batteries, on which the battery-based ESS is dependent [4]. On the other hand, another vital index is the voltage response of the battery, which is required for the co-design and co-simulation with other devices in the practical system. We have developed two online non-invasive SOC and SOH co-estimators for Li-ion battery and the detailed descriptions would be published elsewhere. This study is emphasized on the prediction of SOE and voltage responses of Li-ion batteries with known SOH and initial SOC, considering dynamic load and battery ageing conditions.

SOE allows a direct determination of the residual energy state of batteries. Rigorous and intuitional SOE estimation can further help to predict the battery runtime, which is of the

foremost concern for ESS applications. Traditionally, SOC was the default index descriptive of the available energy state of batteries. In the literature, a wide variety of SOC estimation approaches had been reported, such as the coulomb counting method [5], the OCV-based method [6], and methods based on unscented Kalman filter (UKF) [7], sliding-mode observer [8], proportional integral [9], neural network [10], and fuzzy logic [11], and most of them achieved remarkable results. However, since SOC represents the capacity state instead of the energy state, it is no longer sufficient to describe the battery behavior in the ESS applications where the residual energy rather than the residual capacity of batteries is essential [4]. SOE was introduced in 2010 to directly delineate the energy state of batteries [12, 13] and the detailed review and the differences between SOE and SOC will be discussed in Section II.

Compared to the SOC estimation, there existed only a few literatures on SOE estimation. Mamadou et al. advocated the criterion of SOE in [12, 13] to evaluate the residual energy state of batteries directly, and presented the follow-up algorithms for SOE prediction based on power-integral method. Nevertheless, the disadvantage of the algorithms was the significant estimation inaccuracies caused by the erroneous measurements and the rate capacity/energy phenomenon of batteries. In [4, 14], neural networks were used to predict the battery SOE variation, but the estimation exactness highly depended on the training data provided and the systematic complexity needed to be decreased to reduce the hardware costs. Some researchers tried to extract the relationship between SOC and SOE and several algorithms were developed accordingly. For example, Wang et al. proposed a joint algorithm for SOC and SOE co-evaluation with the aid of particle filters (PFs) in [15] and Bayesian learning technique in [16], Zheng et al. [17] investigated the SOE trajectory with respect to SOC and presented a quantitative relationship between SOC and SOE, and the estimation results were verified under both constant and dynamic load conditions. However, the SOE estimation accuracy of these algorithms were totally dependent on the estimated SOC results, and the estimated SOE results were merely verified at load current of no more than 1.0 C. Other online SOE estimators included the Gaussian model-based data-driven filter [18], and filters based on UKF and recursive least square (RLS) [19], adaptive unscented Kalman filter (AUKF) [20], and dual filter consisted of extend Kalman filter (EKF) and PF [21]. These online estimators achieved acceptable results, but the intricate filtering algorithm produced heavy computational burdens for the micro-processors in the BMSs, which were always with limited computational capability. Additionally, Lin et al. [22] proposed a multi-model-probability-based approach to jointly estimate the battery SOE. Be that it might be, the weights of each model were kept the same under dynamic loads for simplicity, resulting in that the SOE estimation results achieved little improvement.

All of the cited SOE estimation approaches have their own pros and cons. However, there still exist some common drawbacks. Firstly, to date there is no unified determining equations for SOE. Although SOE was defined for the first time in [12, 13], it is still facing the shortcomings of not being clear and practical enough. What's worse, most studies failed to obtain desirable SOE estimation against varying loads, ambient temperature and battery ageing conditions. In the course of battery ageing and operational condition variations, the non-adaptive pre-set model parameters would cause the predicted SOE values deviated from the accurate ones. Last but not least, unfortunately, all of the above-mentioned research works only focused on the estimation of SOE but did not involve the prediction of the voltage responses of batteries: in the online SOE estimators [15-21], the voltage responses were taken as input factors. It should be noted that in the practical smart grid applications, batteries operated together with other electrical devices such as diesel generators, PV plants and domestic loads closely [23]; therefore, it is essential to systematically predict the online voltage responses of the batteries along with the SOE, with an aim to achieve higher compatibilities for the co-operation and co-design with other devices in the smart grids applications.

To compensate the foregoing drawbacks, a comprehensive hybrid Li-ion battery model is advocated in this paper, which is capable of predicting the online battery SOE as well as the voltage characteristics accurately under various operating loads and battery ageing conditions. In addition, the effects of the battery operational conditions such as load current, initial state, ambient temperature and ageing levels are systematically scrutinized and involved into the proposed model. Another improvement is that the proposed model can predict the SOE and terminal voltage of the battery from any starting states, comparing to that most models in the literature were only verified from the fully charged state of batteries. Furthermore, the effectiveness and robustness of the proposed estimator is evaluated and validated by the laboratory-scale test results on commercial $Li_4Ti_5O_{12}$ (LTO) battery cells.

The reminder of this paper is organized as follows. Section II summarizes the related work and Section III elaborates the experimental setup, the proposed model and the workflow. Section IV presents the model extraction process, and the obtained parameter values of the proposed battery model are illustrated and discussed in Section V. Section VI validates the efficacy of the proposed model for predicting SOE and terminal voltage under dynamic loads and arbitrary battery ageing conditions. Finally, Section VII concludes the paper and the future work is addressed.

II. Related Work

A. Electrical Circuit Battery Model

Being the most intuitive and facile to handle, electrical circuit models (ECMs) have been pervasively used in circuit simulators and alongside applications, and they are among the most suitable candidates for battery parameters and terminal voltage prediction. Most of the ECMs can be sorted as impedance-based [24, 25] or Thevenin-based models [25-29]. However, the essential usage of the electrochemical impedance spectroscopy (EIS) scan in frequency domain of the impedance-based models caused them less applicable in the

practical smart grid applications. On the other hand, the Thevenin-based models were mainly extracted via the pulse charge (PC) and pulse discharge (PD) tests [25-29].

In this study, the 2nd order RC Thevenin-based model is chosen. Theoretically, all of the model parameters are multi-variable functions of SOC, current direction and rate, ambient temperature, self-discharge rate, hysteresis effects, and ageing levels of the batteries. A parameter identification method was presented by Hentunen et al. in [28] and it had been widely accepted and utilized in the literature. However, some enhancements could be implemented during the parameter identification procedure. In this work, a revision is proposed to the method in [28] and a novel model extraction method is presented accordingly to realize more thorough and accurate parameter extraction results for the 2nd order RC battery models. Additionally, due to the intrinsical peculiarities of ECMs, there is some deficiency in capturing the non-linear battery behaviors induced by the load variations and will undermine the SOE estimation accuracy if ECMs work alone under strenuous loads. Several hybrid models [30-33] provided viable solutions to describe the non-linear behaviors of batteries.

B. State of Energy

SOE allows a straightforward description of the available energy state of batteries, which is paramount for the energy deployment and optimization in the smart grid applications. As reviewed by Liu et al. [4], SOE outperformed SOC in denoting the residual energy of power-battery-based ESSs, of which the BMSs appeared an ever-growing more sophisticated tendency. SOE was directly linked to the attainable energy of the battery, while SOC focused on the capacity. SOC changed with the discharging current, but the battery energy was the product of the voltage and capacity. The battery voltage decreased in the course of discharge, but the internal energy loss and the energy efficiency of the battery were not considered in the SOC estimation [4, 34]. At the same SOC, SOE varied on account of that the discharging energy efficiency was dependent on the battery operating conditions. Some research works in the literature derived relations between SOE and SOC [17] and the OCV-SOE characteristics [16-19, 22], however, tests results in the current study revealed that there was no robust relation between SOE, SOC, nor OCV. Consensuses were achieved with the inference of [4, 35].

In principle, SOE was defined by the ratio of the residual available energy (RAE) over the maximum available energy (MAE) of the batteries, where RAE denoted the energy that could be retrieved from the battery at an arbitrary initial state when it was discharged down to the lower voltage threshold, and MAE indicated the overall dischargeable energy of a fully charged battery. Upon its advent, power-integral methods were advocated to calculate the online SOE of batteries [12, 13]. However, the facts that the battery discharging performance was greatly dependent on the operating conditions would lead to the power-integral method insufficient to capture the accurate SOE during discharging. The battery SOH, ambient temperature, and load conditions would all influence the discharging performance thus inducing quantitative change of RAE and MAE and further the SOE. Therefore, in the pursuit of a rigorous and accurate SOE estimation, the varying operating conditions of the battery needed to be scrutinized.

In the literature [4, 14-22], focus was purely on ΔSOE, which was the SOE increment/decrement during a time interval, while the initial SOE, the RAE and MAE were scarcely considered. Using ΔSOE could help to set up the state-space equations employed in the filters. However, due to the omission of the initial SOE, the estimated SOE of the online filters based on, for example AUKF [19, 20] and dual filters [21], remained diverged until 10 minutes after the estimation started. This would definitely yield troubles for the instantaneous SOE estimation and might lead to irreparable issues in practical applications. In seeking to address this defect, direct focus is put on the initial SOE, the RAE and MAE of the batteries under various load conditions in the current study. Li et al. [35] demonstrated a preliminary investigation on the effects of ambient temperature and current rate on the battery discharging performance and the online SOE. Moreover, in this study, the effects of another critical index of batteries, the SOH, along with other influencing factors for the online SOE and the battery discharging performance are analyzed more thoroughly.

C. State of Health

Ageing effects commonly appeared amid Li-ion batteries. SOH reflects the degradation extent of the battery capacity as battery ages, and it is of paramount significance in practical applications. The major ageing mechanisms of Li-ion batteries include the loss of active material (LAM), loss of lithium inventory (LLI), and the increase of impedance [36]. In addition, there are basically 2 kinds of battery ageing, namely, calendar-ageing and cycling-ageing [37]. Nevertheless, based on our test results published elsewhere and in [37], the calendar-ageing caused negligible effects on the battery performance, thus only the cycling-ageing effects were considered in this study. Interested readers are referred to our other publications focusing on the online SOH and SOC co-evaluations of batteries. Herein we assumed that the SOH and initial SOC were already known. Moreover, according to our experimental results and that in [38], the extent of the cell degradation in capacity was not correlated with the ageing or cycling conditions. Therefore, in this study, accelerated aging tests at 3.0 C and 55 °C were conducted to prepare batteries with various SOHs. A fresh cell and 3 aged cells with known SOHs were tested separately, and an aged cell with an arbitrary SOH was used for model validation.

III. Experimental Set-up and Test Procedure

A. Test Bench Scheme

The basic parameters of the tested LTO battery are listed in Table I. With the ability to carry large current and withstand a wide range of temperature, LTO batteries are more inclined to the ESS applications. A test bench was built for data acquirements as shown in Fig. 1. It consisted of a battery tester, a temperature chamber, and a host PC to control the tester and to record the test data. The deployed BMS and CAN were within the tester for protection and data collection and transmission purposes. 1 mV precision was for voltage measurement and 1 mA for the current. The thermal chamber

TABLE I
BASIC PARAMETERS FOR THE LTO BATTERIES USED FOR TESTS

Battery Parameter	Characteristics
Nominal capacity	20.0 Ah
Nominal voltage	2.3 V
Charge condition	CC-CV 2.7 V 20.0 A, 1.0 A cut-off
Discharge condition	CC 6.67A, 1.5 V cut-off
Operating temperature	-30 ~ 55 °C

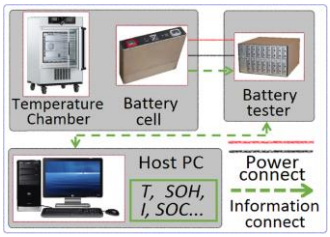

Fig. 1. Test bench schematic.

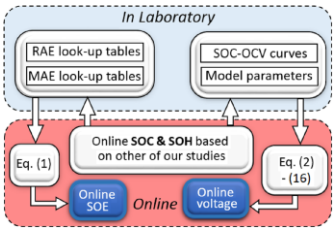

Fig. 3. Proposed model workflow.

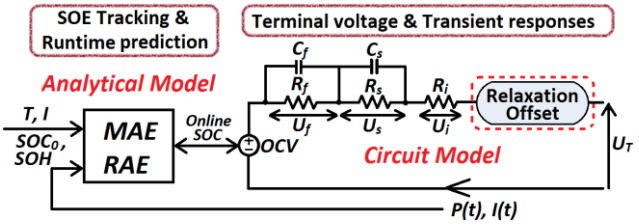

Fig. 2. Proposed battery model.

kept the batteries operated under designated ambient temperature. All the data were input into Matlab/Simulink.

B. Proposed Model and Workflow

In this study, we aim to set up a practical Li-ion battery model to bridge the gap between laboratory test results and real-life smart grid applications, so that the laboratory test data could be used to predict the anticipated Li-ion battery performance in practical applications. The proposed hybrid battery model was built in Matlab/Simulink. As shown in Fig. 2, it comprised an ECM on the left which was responsible for the terminal voltage and transient responses tracking, and an analytical model on the right for SOE and runtime prediction. The two models were conjugated by the online SOC. There were 7 components in the ECM: open circuit voltage (*OCV*), R_i and 2 polarization RC network combinations, namely, R_f, C_f, R_s and C_s, and a relaxation voltage offset component U_{offset}. R_i was the ohmic resistance of the battery and consisted of the surface layer resistance and the bulk resistance, and it was responsible for the instantaneous voltage drop and rise. R_f and C_f modeled the fast dynamics such as activation polarization and τ_f was the fast time constant with a typical value of seconds. R_s and C_s represented the slow dynamics in the order of tens of seconds or minutes, and they were more representative of the concentration polarization. τ_s was the slow time constant. U_{offset} captured the long-term battery behavior during idle periods, and its value was zero when the battery was loaded. *OCV* was the voltage of fully relaxed battery and U_T was the terminal voltage of the battery. Compared to other 2nd order RC ECMs [25-29, 39], U_{offset} is introduced herein to encapsulate the long-term battery voltage relaxation characteristics for improving the model fidelity.

The analytical model for SOE and runtime prediction aimed at involving the multidimensional quantitative dependence of the MAE and RAE values of batteries on current rate, ambient temperature, SOH, and the initial SOC as a holistic database, where MAE and RAE were outputs and other operational variables acted as inputs. Based on the literature review and to the best of the author's understanding on the index of SOE, we advocated the SOE determination equation as:

$$\mathrm{SOE}(x\%) = \frac{E_{RAE|I,T,SOC,SOH}}{E_{MAE|I,T,SOH}} \times 100\% \quad (1)$$

The denominator was the MAE value of the battery by depleting a fully charged battery of a particular SOH $z\%$ under the designated current rate I and ambient temperature T. The numerator was the RAE but with the initial SOC as another factor to consider, and it was acquired via fully discharging the battery with $z\%$ SOH and a certain initial SOC $y\%$ at I and T. The values of MAE and RAE under each condition were calculated via the power-integral method. This proposed SOE determination approach took thorough consideration on all the influencing factors on the discharging performance and further the online SOE of batteries. With the help of (1) and the database in the analytical model, the proposed model was capable of achieving high-fidelity SOE estimation under varying operational condition and SOH levels.

The overall workflow of the proposed model was illustrated in Fig. 3. First of all, based on the model parameter extraction approach proposed in this study, the OCV-SOC characteristics and model parameters of the battery such as R_i, R_f, C_f, R_s, and C_s at each I, T, SOC and SOH were extracted offline in the laboratory and multidimensional look-up tables for each battery parameters were set up accordingly. Details of advocated methodology would be given in the next section. Meanwhile, multidimensional look-up tables for RAE and MAE with respect to each of the influencing factors were built offline as well. When the online SOC and SOH of the battery were identified through our online SOC and SOH co-estimators, and the operating conditions were collected by the testers, they were all input into the proposed battery model. Additionally, the online SOC was obtained via coulomb counting method during battery operations. The online values of the model parameters, RAE and MAE of the battery would be simultaneously available via the interpolations in the implemented look-up tables, thus the online voltage responses, SOE, and runtime of the batteries would be immediately attainable. This proposed generic modeling method was concise but useful since it allowed accurate online prediction of battery performance using data gleaned from the laboratory-scale tests.

IV. MODEL EXTRACTION

In this section, the model extraction procedures were elaborated. The battery parameters were obtained at 5 ambient temperature, 5 °C, 15 °C, 25 °C and 35 °C and 45 °C. Meanwhile, the selected SOHs were 100%, 95%, 90%, and 85%, in correspondence to battery capacity of 20.0 Ah, 19.1 Ah, 18.1 Ah and 17.0 Ah.

Let us first look at the analytical battery model. MAE look-up table was determined by depleting a fully charged battery (charged via the rated CC-CV approach as specified in

Table I) at 0.33 C, 0.5 C, 1.0 C, 1.5 C, 2.0 C, 2.5 C, 3.0 C, 3.5 C, 4.0 C, 4.5 C and 5.0 C, separately. The look-up table for RAE was acquired in an analogous way and the corresponding initial SOCs were of 5%, 10%, 20%, 30%, 40%, 50%, 55%, 60%, 70%, 80%, 90%, and 95%, separately (the initial SOC were obtained by discharging fully charged batteries at 0.33 C for an associated period according to SOH, as stipulated by the battery manual). After the values of battery MAE and RAE with respect to each of the influencing factors were extracted, the analytical model was built accordingly.

Furthermore in this paper, a novel parameter extraction method and procedure for the electrical circuit model were specified.

A. Proposed Parameter Extraction Method

A PC/PD test conducted on a fresh battery cell at 1 C and 25 ºC was demonstrated to exemplify the proposed method. The cell was first relaxed in the temperature chamber for 4 hours to reach equilibrium before fully discharged at 0.33 C. The cell was relaxed for 2 hours and was fully charged in the rated manner, and then completely depleted at 0.33 C after a 2-hour rest. The first cycle ascertained the actual capacity and the SOH of the battery cell. The cell was again fully charged and the PC/PD tests began.

- Constant current (CC) PC (I > 0) of 3.0 C with duration of 10 s and sampling time 0.02 s. A steep voltage increase was observed. R_i of the charge direction was calculated using the step voltage increment.
- 5 min relax period between the PC and PD tests.
- CC PD (I<0) of 3.0 C with 10 s duration and sampling time 0.02 s. An abrupt voltage fall appeared as anticipated. R_i of the discharge phase was calculated by the step voltage decrement.
- 5 min rest after pulse injections.
- 72 s CC discharge with 1.0 C to reduce the SOC by 2% (within SOC ranges of 90%-100% and 0%-10%), or 180 s galvanostatic discharge at 1.0 C to reduce the SOC by 5% (for the 10%-90% SOC range). The data was sampled at 1.0 s.
- The cell was rested for 2 hours after each load to reach equilibrium before the next test began. During these intervals, the current was zero and the SOC was a constant value. The data was sampled at the highest time resolution of 1.0 ms as it was used for calculation of the transient impedance parameters and the data quality needed to be good for high precision.

The pulse characterization tests were cycled until the cell voltage reached 1.5 V. The processes were then repeated in the charge direction. Fig. 4 showed the *V-I* trajectory of the cell under the tests. The same test profile was repeated for 0.5 C, 2.0 C, 3.0 C and 4.0 C SOC reduction and increment characterization on cells with the other 3 SOHs and other 4 ambient temperatures. For all the tests, the current rate of PC and PD tests were kept at 3.0 C, and the parameters of the ECM at each operating condition were extracted from the respective pulse test characterization results.

B. Extraction of Internal Resistance

A magnified *V-I* plot with relaxation phase from Fig. 4 was shown in Fig. 5 to elaborate the advocated method for

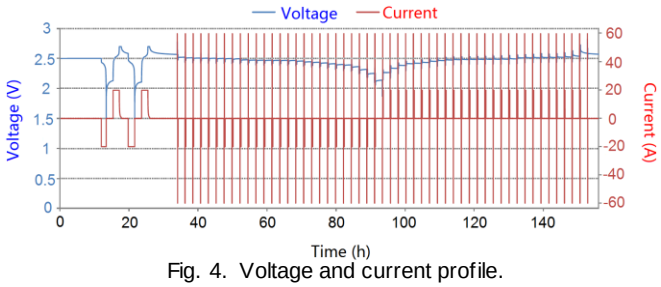

Fig. 4. Voltage and current profile.

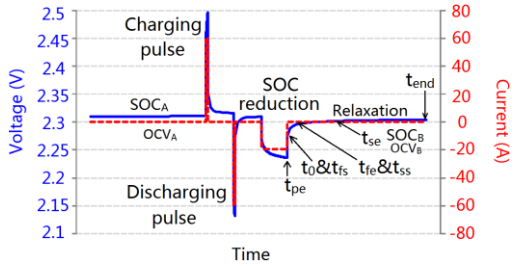

Fig. 5. Zoomed V-I profile during PC and PD tests.

parameter calculation. Initially, the cell was in equilibrium at SOC_A. The 3.0 C PC was injected for 10.0 s, which increased the cell SOC by:

$$\frac{60.0\,A \times 10\,s}{3600\,s/h \times 20.0Ah} \times 100\% = 0.833\%$$

thus, the SOC of the cell was at SOC_A + 0.833% after the PC injection. This subtle SOC change had to be accounted for when calculating R_i values at pulse injections so that the correct R_i values at the relevant SOCs could be obtained. When the cell was injected with the 3.0 C PD with a duration of 10.0 s, the SOC of the cell reverted back to SOC_A. This was followed by a 1.0 C CC discharge, after which the cell was in relaxation state at SOC_B, as illustrated in Fig. 5. R_i values were calculated and benchmarked from the instantaneous voltage drop and rise during the pulse tests as well as the switch on and off phases of each 3.0 C PC/PD test in the course of both charge and directions. R_i was determined by:

$$R_i = \frac{V_0 - V_1}{I} \tag{2}$$

where V_0 was the cell voltage at the start of the pulse injection at t_{pe}, and V_1 was the voltage 1 s after at time t_0, when the pulse current had reached zero, as shown in Fig. 5. I was the injected current rate, positive for charge and negative for discharge. R_i was also calculated in the SOC reduction and increment phases of 0.5 C, 1.0 C, 2.0 C, 3.0 C, and 4.0 C at various SOHs and temperatures. The results would be presented and discussed in Section V.

C. Extraction of Impedance Parameters

It was more appropriate to calculate the values of the impedance parameters from the relaxation phases of the cell where the SOC was constant and the load current was zero. In the proposed model, the voltage relaxation offset, U_{offset} was introduced to encapsulate and better describe the long-term voltage relaxation characteristic, in addition to the fast and slow dynamic voltage elements. The proposed time window divisions of the relaxation period were shown in Fig. 5: t_0 was the starting time of the relaxation period, which was the same as the starting time for the fast dynamic, t_{fs}. U_f denoted the voltage of the fast dynamic. t_{fe} was the ending time of the fast dynamic,

where U_f decayed to the vicinity of zero. t_{ss} was at the same point with t_{fe}, and it was the time when the slow dynamic began to dominate. U_s indicated the voltage of the slow dynamic. t_{se} was the time when U_s had approached zero, after which time epoch the transient voltage only consisted of U_{offset}. The end of the relaxation period was marked by t_{end}, which was basically 2-hour later of t_0 and right before the next pulse current injection. U_i was the ohmic over-potential due to R_i, therefore:

$$U_i(t) = I(t)R_i \quad (3)$$

The terminal voltage of a loaded cell was represented by:

$$U_T(t) = OCV + U_f(t) + U_s(t) + U_i(t) \quad (4)$$

When the battery was switched from loaded to relaxed condition, the load current became zero and U_i disappeared immediately. The battery did not reach equilibrium at once because the internal electrochemical reactions took some time to decay. The battery terminal voltage during relaxation period $t_{fs} - t_{fe}$ became:

$$U_T(t) = OCV + U_f(t) + U_s(t) + U_{offset}(t) \quad (5)$$

Similarly, in the time of $t_{ss} - t_{se}$, U_f had decayed into the vicinity of zero thus could be ignored, and the battery terminal voltage was:

$$U_T(t) = OCV + U_s(t) + U_{offset}(t) \quad (6)$$

When U_s approached zero during $t_{se} - t_{end}$, U_T equaled to:

$$U_T(t) = OCV + U_{offset}(t) \quad (7)$$

Finally, in fully equilibrium state after t_{end}, U_T equaled to OCV:

$$U_T(t) = OCV \quad (8)$$

Fig. 6 was re-plotted from Fig. 5 with various voltage elements. $U_{offset}(t)$ was the voltage difference from t_{se} to t_{end}, and its maximum value was around 8 to 15 mV in a time frame of 1 to 2 hours empirically. This subtle voltage change after 1.0-hour relaxation time was usually not paid with enough attention in the literature [26-30]. In this study, U_{offset} was introduced and modeled as an additive linear function of relaxation time beyond t_{se} by choosing τ_f and τ_s appropriately. This would increase the model accuracy but keep the additional increase of the computational complexity to a minimal level. $U_{offset}(t)$ was then calculated from the voltage difference between t_{se} and t_{end} in the general form as:

$$U_{offset}(t) = \frac{Relaxation\ \ Offset}{t_{end} - t_{se}} \times t, \text{ for } t_{se} \le t \le t_{end} \quad (9)$$

In this study, we presented a novel method to separate U_f, U_s, and U_{offset}. Fig. 7 showed the typical transient voltage responses within the idle period after pulse charging. U_f was illustrated in green color, and U_s and U_{offset} in red and black, separately. The blue curve delineated the values of the battery terminal voltage subtracting the OCV, $U_T - OCV$, which was actually the transient voltage. Based on the foregoing discussions, the transient voltage was cast up by U_f, U_s and U_{offset}. However, these 3 components were not existed all concurrently throughout the whole idle period. In order to separate U_f, U_s and U_{offset}, the derivative of the transient voltage with respect to the elapsed time was calculated for the entire idle period, as illustrated in Fig. 8. D_f, D_s and D_{offset} were the derivation of U_f, U_s and U_{offset}, respectively. Since U_{offset} was modeled as a linear expression in this study, D_{offset} was a constant. The time epoch of t_{se} was identified during the latter part of the 2-hour idle period empirically (approximately between 50-80 minutes), when the evolution of the voltage derivation was larger than 0.1 mV•(s•min)$^{-1}$ (i.e., when the voltage derivative was larger than

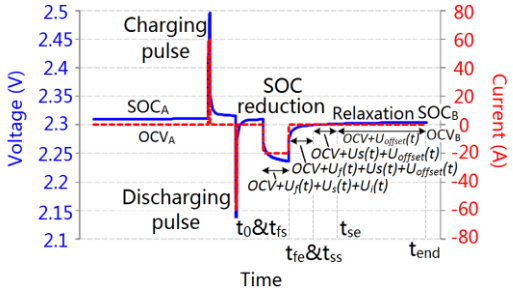

Fig. 6. Pulse profile with various voltage component.

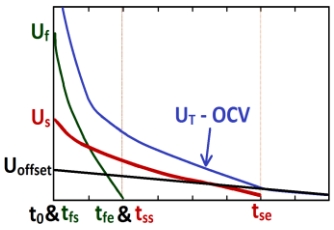

Fig.7. Voltage elements during battery relaxation period.

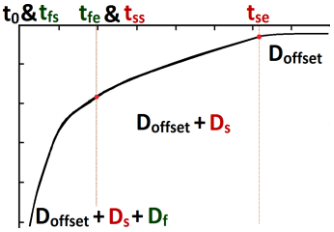

Fig.8. Derivation of the transient voltage U_T - OCV.

4 mV• s^{-1} compared to that at time t_{end}), therefore, the average of the voltage derivation between t_{se} and t_{end} was assigned as D_{offset}. After subtracting D_{offset} from the derivation of the transient voltage, the remaining parts from t_{fs} to t_{se} was composed of two exponential functions, D_s and D_f, but D_f dropped into the vicinity of zero at a time epoch between t_{fs} and t_{se}. A short period closely before t_{se} (typically 10-15 minutes) was chosen for curve fitting to identify D_s and to determine t_{ss} and t_{fe}, then D_f was obtained by subtracting D_s and D_{offset} from the derivation of the transient voltage. Through this advocated approach, the value of D_s, D_f, D_{offset}, and the time epochs of t_{fe}, t_{ss} (t_{fe}), and t_{se} could be determined. Furthermore, in light of that U_f and U_s were both in exponential form, the time constants of the fast and slow dynamics, τ_f and τ_s, could also be identified. Because the fast and slow dynamics were both modeled as RC combinations, the following expressions could be stated:

$$U_s(t) = U_s(t_{ss}) \times e^{-\frac{t-t_{ss}}{\tau_s}} \quad (10)$$

$$U_s(t) = U_s(t_0) \times e^{-\frac{t-t_0}{\tau_s}} \quad (11)$$

where $U_s(t_{ss})$ and $U_s(t_0)$ were the voltage of the slow dynamic at time t_{ss} and t_0, separately. By substituting $U_s(t_{ss}) = U_T(t_{ss}) - OCV(t_{ss}) - U_{offset}(t_{ss})$, the value of $U_s(t_0)$ was given as:

$$U_s(t_0) = [U_T(t_{ss}) - OCV(t_{ss}) - U_{offset}(t_0)] \times e^{-\frac{t_0 - t_{ss}}{\tau_s}} \quad (12)$$

Thus $U_f(t_0)$ could be calculated as:

$$U_f(t_0) = U_T(t_0) - OCV(t_0) - U_s(t_0) - U_{offset}(t_0) \quad (13)$$

where $U_s(t_0)$ and $U_f(t_0)$ were the values of the slow and fast dynamic voltage elements at time t_0, when the load current had fallen to zero and the voltage transient processes took place. Mathematical expressions of $U_f(t)$ and $U_s(t)$ could be drawn as:

$$U_f(t) = U_f(t_0) \times e^{-\frac{t-t_0}{\tau_f}}, \text{ for } t_0 \le t \le t_{fe} \quad (14)$$

$$U_s(t) = U_s(t_0) \times e^{-\frac{t-t_0}{\tau_s}}, \text{ for } t_0 \le t \le t_{se} \quad (15)$$

Since t_{pe} was only 1.0 s before the time of t_0, we could assume that the expression in (14) and (15) were also applicable at t_{pe} when the load current just started to fall. Therefore, the value of impedance parameters R_f, R_s, C_f, and C_s could be calculated as:

$$R_n = \frac{U_n(t_{pe})}{I(t_{pe})} \quad (16)$$

$$C_n = \frac{\tau_n}{R_n} \quad (17)$$

where $n = f$ or s. With the help of the proposed method, the parameters of the 2nd RC circuit model at each SOH, T and I could be identified. The parameters extraction results of the ECM and the discussions were detailed in Section V.

D. Innovation and Enhancement of Proposed Method

In this study, we advocated a novel parameter identification method for the 2nd RC ECM, as a modification to the method in [28] in order for realizing more thorough and precise parameter extraction results. In specific, there were 4 aspects of innovation and enhancements compared to the previous methods. Firstly, when complying with the method proposed in [28], we initially encountered difficulties in selecting the time windows according to the length of the idle period between current pulses and the partitioning requirements stipulated in [28] that, the starting time for the slow time window should be later than three times of the fast time constant [28]. The short idle period of 5-60 minutes stipulated in [28] restricted the process when we tried to identify the time windows following the instruction. As a result, in this study, we turned to select two adjacent time windows to extract the ECM parameters more intuitively. In supplement, due to the fact that there was still some voltage variation after 1 hour's rest in the idle period, the interval of the rest time between current pulses was advocated to be 2 hours, instead of the short idle time of 5-60 minutes. This prolonged rest time guaranteed the battery to completely reach equilibrium thus the entire transient voltage could be captured, and the accuracy was improved. Secondly, the subtle transient voltage variation after the fast and slow dynamics was ignored [26-28], or considered as another RC branch [17], or as electrochemical elements [30-32] in the literature, which either caused the defects on precision or being too complicated. We introduced a linear voltage elements U_{offset} to represent the subtle transient voltage change after the fast and slow dynamics to rectify this drawback. Thirdly, the pulse test profile was optimized, and R_i values were calculated at a higher resolution from more SOCs in both charge and directions and switch on/off phases. Furthermore, in (22) of [28], R_f and R_s were calculated by the V-I values of time t_0. Nevertheless, both [28] and our work defined t_0 as the time when the pulse current had fallen to zero, so it was inappropriate to calculate R_f and R_s at t_0. In this work, we advocated (16) and (17) for R_f and R_s through the V-I values at t_{pe} instead, when the pulse current just began to fall. Last but not least, the influences on battery behaviors of temperature, current rate and direction, and ageing levels were involved in the model. This proposed approach had good generality and were highly versatile to simulate any cell materials without deep insights into the chemistry itself. In conclusion, the proposed method was capable of improving the model accuracy and offering a good trade-off between the model accuracy and computational burden.

V. Parameter Extraction Results

A. OCV-SOC Characteristics

The batteries used in this study had hysteresis of no more than 2 mV [31-33] and were cycled regularly, thus hysteresis and self-discharge were ignored without any noticeable effects on model accuracy. The OCV-SOC characteristics were extracted at various T and SOH, and the OCV-SOC curves of the fresh cell (20.0 Ah) and the most aged cell (17.0 Ah) under 5 °C, 25 °C, and 45 °C were illustrated in Fig. 9 for clarity. The curves were identified via the rapid method presented in [27] and the markers were acquired by measuring the battery voltage after 2 hours' relaxation. Fig. 9 revealed that higher T resulted in a wider OCV range. Additionally, OCV of the same SOC was lower as battery aged, and more OCV decrements were observed when SOC was larger than 40%.

B. Analytical Model Extraction Results

The analytical model extraction results were illustrated and discussed in this part. Fig. 10(a) depicted the MAE dependence on I and T. At same T, MAE decreased with increasing I. For instance, at 5 °C, MAE dropped from 41.26 Wh to 38.12 Wh when I changed from 0.33 C to 3.0 C. Meanwhile, MAE exhibited an increasing tendency with rising T. Fig. 10(b) showed the MAE trajectory with SOH: when 0.33 C and 25 °C were chosen, MAE was 46.59 Wh for fresh cell, and 44.78 Wh, 42.1 Wh and 37.9 Wh for each aged cell, respectively. In addition, the monotonic decreasing trend of I on MAE was also discovered, albeit at different SOHs. Summary could be drawn that MAE was greatly affected by T, I and SOH.

The only distinction of RAE from MAE was that the initial SOC was not 100%, hence it was plausible to speculate that RAE conformed to the similar dependence trend of MAE on T and SOH. Fig. 11 illustrated a 3-D representation of RAE variation on initial SOC and I of a fresh cell at 25 °C. The red dots and the yellow squares represented the RAE values at various I from 100% and 40% initial SOC, respectively. The values were listed in Table II and the ratio of the two sets of RAE at same I was also obtained. It could be extrapolated that the larger was the current, the lower was the ratio; thusly, summary was that at the same SOC, SOE varied when I was changed, which corroborated the deficiencies of the models in [15-17] where SOC-SOE linear relations were built. The analogous 3-D RAE representations for other T and SOHs were also set up. With the comprehensive involvement the influences of I, T, initial SOC, SOH on battery MAE and RAE into the database, the proposed model could realize high-fidelity SOE estimation against varying load and battery ageing conditions.

The inevitable energy loss of the battery due to the dynamic loads could be the results of either reversible or irreversible energy loss. Our previous study proved that there was net energy loss of batteries ascribed to large discharge current and it was irreversible unless the battery was fully re-charged. On the other hand, the reversible energy loss was due to the rate energy effects and recovery effects [30, 33]. However, in this study, the irreversible and reversible energy loss were not discussed, and we only considered the battery RAE and MAE when discharged under a designated load condition. Future study would explore more about the energy loss and took the idle time into consideration to track the recovery rate of the batteries under dynamic load conditions.

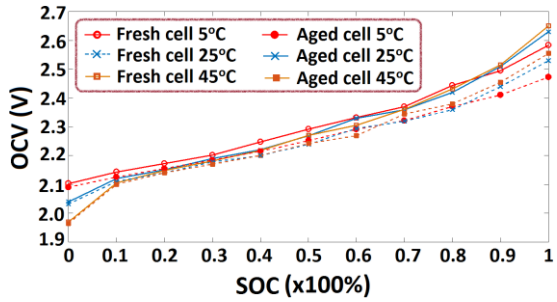

Fig.9. OCV-SOC relation with temperature and ageing effects.

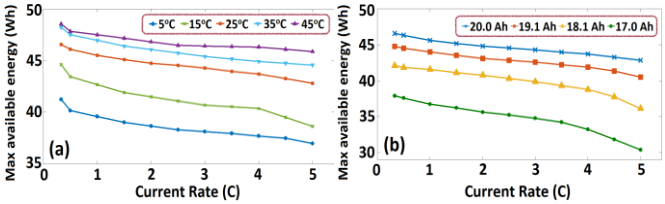

Fig.10. MAE dependence on *I* at various (a) *T*, and (b) SOH.

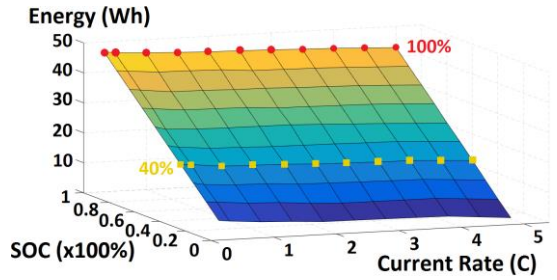

Fig.11. 3-D representation of RAE variations with initial SOC and *I*.

TABLE II
RATIO OF THE RAE VALUES AT 40% WITH THAT OF 100% INITIAL SOC AT VARIOUS LOAD CURRENT (100% SOH, 25 °C)

I	0.33C	1.0 C	2.0 C	3.0 C	4.0 C	4.5 C	5.0 C
40%	18.6	17.2	16.8	16.1	15.7	15.2	14.4
100%	46.6	45.5	44.8	44.3	43.8	43.3	43.0
Ratio	40%	38.8%	37.5%	36.3%	35.8%	35.1%	33.4%

C. Electrical Circuit Model Extraction Results

As mentioned above, R_i values were calculated from the switch on and off phases of the 3.0 C PC/PD tests during both charge and discharge situations. R_i values were also calculated at the SOC decrement and increment steps with current rate of 0.5 C, 1.0 C, 2.0 C, 3.0 C, and 4.0 C under each *T* and SOH. Fig. 12 showed the R_i values of a fresh cell at 25 °C calculated from various ways. It could be clearly observed that R_i exhibited a nearly constant value of 10 mΩ within 10-90% SOC range, regardless of the load current rate, switch on/off phases, and charge/discharge situations. Meanwhile, there were abrupt increases in R_i values when SOC approached both 0% and 100%. The simplified plotting of the variation of R_i values on *T* and SOH were shown in Fig. 13. Basically, R_i values increased when the temperature was lower and battery ageing was more severe. Conclusion could be derived that: R_i values were almost irrespective of current rate and direction and switch on/off phases, but depended on SOC, *T*, as well as SOH.

The values of the impedance parameters of the ECM at 25 °C under both discharge and charge regimes with different current rates were shown in Fig. 14-15. In specific, the battery

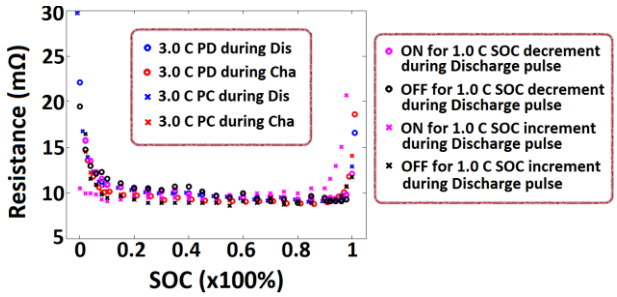

Fig.12. R_i values of a fresh cell at 25 °C from different approaches.

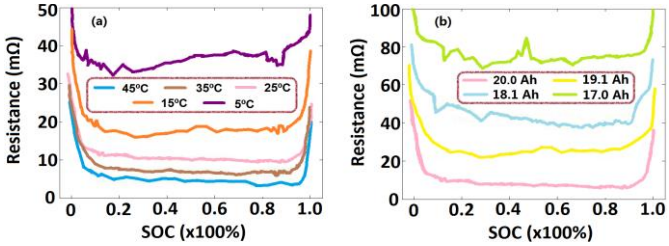

Fig.13. R_i values variation with (a) *T* and (b) SOH.

parameters under discharge denoted the impedance parameters obtained after a discharging event with SOC reduction, while vice versa for the parameters under charging. It could be seen that the parameters under charge and discharge regimes were not equal to each other and they varied with different SOCs and load current rate. For the discharge regimes, the battery voltage drop was more prominent at low SOCs when the cell was almost depleted due to the build-up of concentration gradient, and R_f and R_s became very large due to the slow mass transport and diffusion limitations. In the course of charging events, both R_f and R_s generally increased with the increasing SOC. Meanwhile, R_f and R_s values dropped with increasing current rate, and the values of R_f was slightly larger than that of R_s. As to C_f and C_s, their values were directly related to the current rate and direction. For both charge and discharge regimes, the values of C_f and C_s were larger with higher current rate.

Moreover, Fig. 16 illustrated the impedance parameter values of a fresh cell under 1.0 C discharge regime at different *T*, and the impedance parameter values of 3 aged cells at 1.0 C discharge and 25 °C were plotted in Fig. 17. A downward trend with temperature of R_f and R_s values could be observed, while C_f and C_s generally increased with the rising temperature, and it was more obvious for the values of C_f than that of C_s. From Fig. 17, it could be concluded that SOH exhibited severely adverse effects on the values of the impedance parameters. As the battery aged progressively, R_f and R_s increased on the whole, and the dependence on SOC was more pronounced. Additionally, values of C_f and C_s varied dramatically with SOH in an overall positive relationship.

With the extraction of the parameters of both the analytical model and the electrical model, the proposed hybrid battery model was built in Matlab/Simulink, and the model validation tests began.

VI. MODEL VALIDATION AND DISCUSSION

A. Verification of the Terminal Voltage Prediction

To validate the terminal voltage prediction results of the proposed model, a battery cell with an arbitrary capacity of 18.7

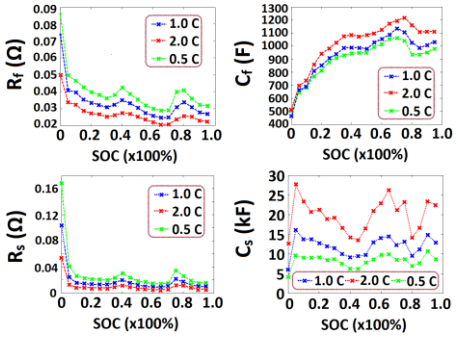

Fig.14. Impedance parameter variations with *I* under discharge.

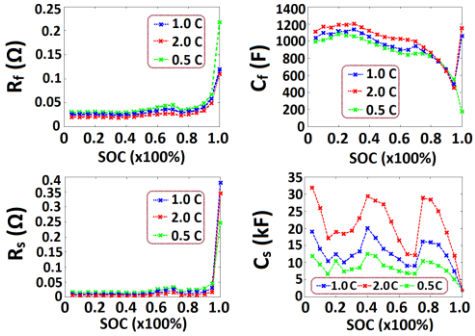

Fig.15. Impedance parameter variations with *I* under charge.

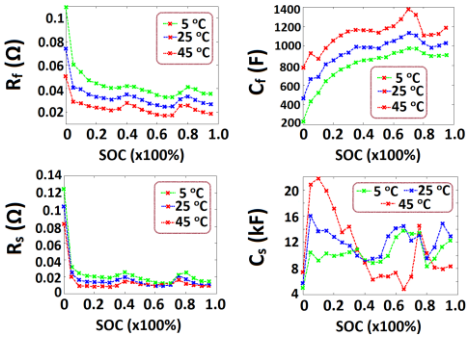

Fig.16. Impedance parameter variations with *T* under discharge.

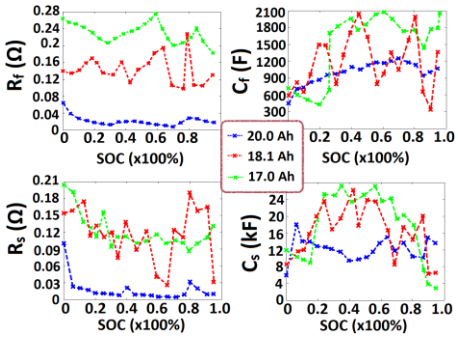

Fig.17. Impedance parameter variations with SOH under discharge.

Ah (commensurate with 93.5% SOH) was fully charged and tested at the load profile shown in Fig. 18 until depleted. The temperature plotting in Fig. 19 was input into the temperature chamber to create varying ambient temperature situations. The simulated voltage results were compared with the voltage measurement from the tester and the results were shown in Fig. 20, where the red line was the simulated voltage and the green line represented the measured one. A close agreement between the two curves could be observed, and the maximum

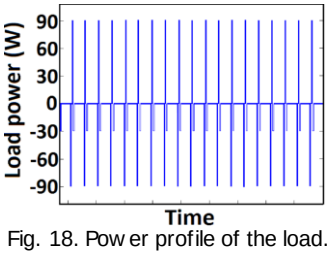

Fig. 18. Power profile of the load.

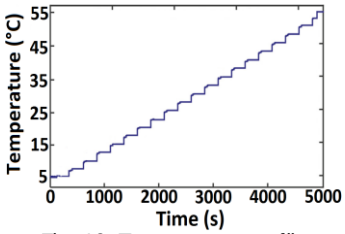

Fig. 19. Temperature profile.

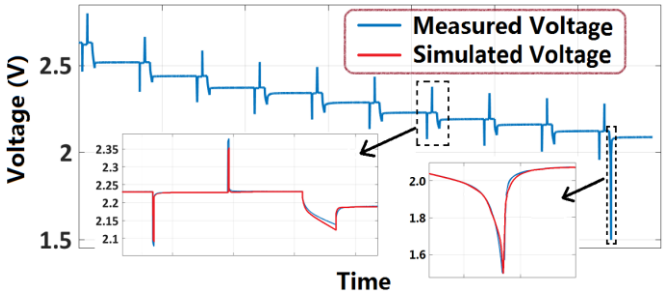

Fig. 20. Comparison of the measured and simulated voltage results.

discrepancy was found at the end of discharge when the cell was nearly depleted (0-10% SOC), where the maximum absolute percentage error (MAPE) was 0.17% and the root mean square percentage error (RMSPE) was 0.23%. In the SOC range from 95% to 10%, MPE was approximately 0.09% and RMSPE was confined within 0.15%. The breakdown of the simulated voltage results with different elements was shown in Fig. 21. The SOC was around 84%. U_i was present during both the charge and discharge events and it was almost constant because R_i varied minimally with SOC and current rate variations. Information could be obtained that, U_f decreased to zero in the course of the relaxation period within a time frame of about 350 s. U_s decayed more slowly in about 2600 s. U_{offset} (about 11 mV), which was modeled as a linear function in the proposed model, decayed much more slowly and vanished in about 1.7 hours.

In the practical smart grid applications, the load was strenuously vibrating and unpredictable. A typical current profile was gleaned from the island smart grid and shown in Fig. 22. The cell for testing was loaded under this highly dynamic current profile from 50% initial SOC for 30 hours to verify the voltage prediction of the proposed model. The comparison of the measured voltage with the simulated one was shown in Fig. 23, where the red curve represented the simulated voltage and the blue curve indicated the measured one. It could be observed from Fig. 22 that the simulated voltage results superimposed very well with the measurements, with the MAPE (found at the 8.5th hour when the online SOC was approximately 12%) less than 2% and the RMSPE of 1.2%.

In the smart grid applications, Li-ion batteries would scarcely be operated below 10% SOC, thus the voltage disparities in this region was of trivial significance. Some BMSs were programmed to discharge the battery no lower than 10% SOC to extend the lifespan of batteries. Even though a battery was discharged below 10% SOC, the errors were acceptably small. Therefore, the proposed model was competent to predict the terminal voltage responses of the battery sufficiently under varying load conditions considering temperature and battery ageing effects.

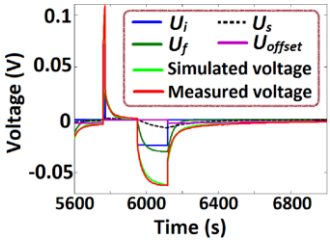

Fig.21. Voltage elements of the simulated voltage values.

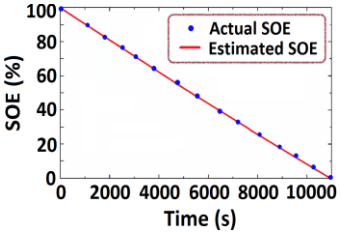

Fig.24. Actual and estimated SOE results under constant *I*.

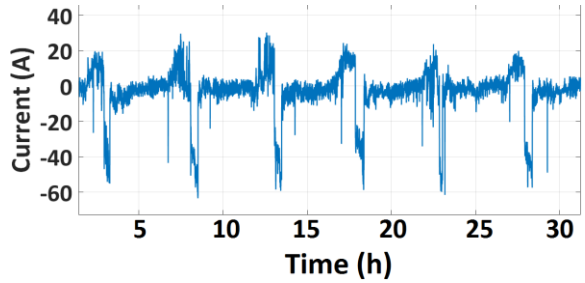

Fig. 22. Dynamic load current profile from the smart grid.

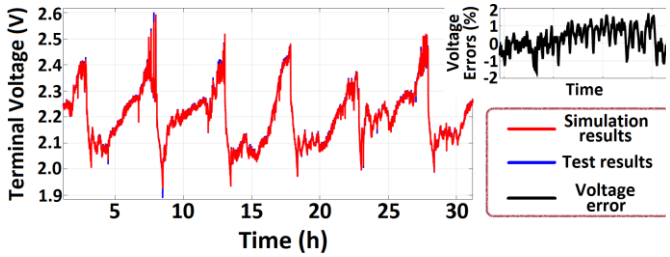

Fig. 23. Comparison results of the measured and simulated voltage.

B. Verification of Battery SOE and Runtime Estimation

In this part, the estimated SOE results of the proposed model were compared with the actual ones. However, to date there was no direct approach for online SOE determination. In the literature, researchers used the power integral method [4] or the Kalman filter [14] to obtain SOE values and declared them to be the actual ones. It was worth noting that SOE results obtained from any algorithms had errors more or less; thus, in this work, the actual SOE values were obtained through brute force according to the determining equation in (1). After the SOE estimation validating tests were finished, the same battery cell was again loaded at the test profile from the same initial SOC and ambient temperature. The tests were cut off discontinuously in a desired time interval of 5 to 15 minutes typically, and the cell was then relaxed for 2 hours before fully discharged at the same current rate before it was manually cut off from the validation test load profile. The dischargeable energy of the cell was the accurate value of the RAE at this point. In supplement, the MAE of the cell was extracted by interpolating the MAE look-up tables in the proposed model according to the online load current rate, temperature and SOH, since MAE was irrespective of the online SOC of the cell. With the values of online RAE and MAE, the actual SOE of the cell was identified through (1). Via this approach, the actual SOE of the cell was obtained one by one at each desired time epochs. This method was a little bit time-consuming, but the results were almost 100% accurate.

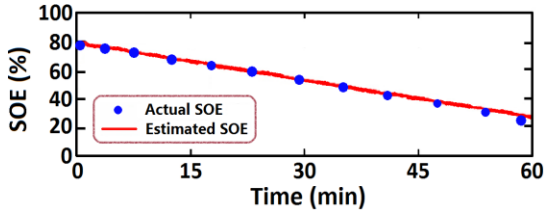

Fig. 25. Actual and estimated SOE under load profile in Fig. 18&19.

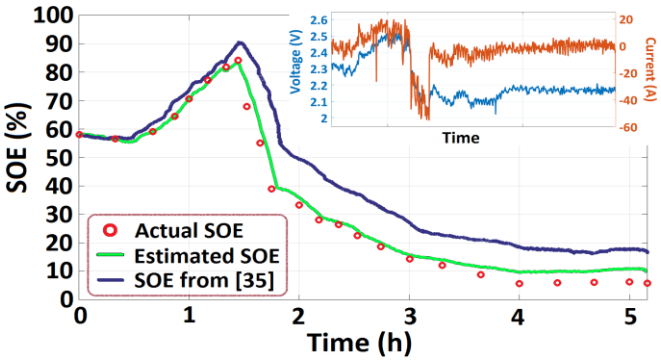

Fig. 26. Actual and estimated SOE results of the proposed model and the model presented in [35] under load profile in Fig. 22&19.

The SOE estimation results of the testing cell at 0.33 C constant current load and temperature profile in Fig. 19 was shown in Fig. 24, where the red line represented the estimated SOE, and the blue dots were the actual SOE values. The MAPE and RMSPE of the estimation results were 2% and 1.1%, and the runtime error was within 1%, revealing that the proposed model performed very well under constant load and dynamic temperature conditions.

In Fig. 25, SOE estimation results under the pulse current load profile of Fig. 18 and temperature profile in Fig. 19 were compared with the actual ones. The initial SOE was 80%. The estimated SOE trajectory was shown in red curve, and the actual SOEs were plotted in blue. During the 1-hour test, good superimposition of the estimated SOE with the actual one could be observed, and the MAPE and RMSPE were 3.2% and 2.1%, respectively.

Additionally, in order to simulate the practical battery operation in smart grid, the model and the testing cell were both loaded at the current profile in Fig. 22 for 5 hours. The initial SOE was 58% and the temperature profile in Fig. 19 was repetitively loaded. Fig. 26 showed the comparison results of the SOE estimation results with the actual ones, and the *V-I* characteristic of the testing cell was also illustrated on the top right corner in Fig. 26. The actual SOE was delineated by red dots, and the estimated SOE was drawn in the green curve. In order to demonstrate the outperformed results for SOE estimation of the proposed model, the SOE estimation results by the model in [35] were also plotted in Fig. 26 in blue. According to Fig. 26, from 0-1.5 h when the load current was moderate (within ±1.0 C), both the SOE estimation could achieve acceptable results, and our proposed model performed slightly better than the model in [35]. From 1.5-5 h when the cell was discharged at current rate of as large as 3.0 C, the estimated SOE from the model in [35] deviated seriously from the actual one, while the SOE estimation of the proposed model was much closer to the actual one. Specifically, the MAPE and

RMSPE of the proposed model were 9.2% and 4.7%, while those of the model in [35] were 26% and 10.9%, respectively.

The test results denoted that the proposed model achieved a significant improvement over the previous model for estimating SOE, and it was capable of predicting the SOE and runtime of an arbitrary aged cell under dynamic load and temperature conditions with high fidelity and reliability. Compared to the model in [35], the electrochemical reactions in the battery at various operating conditions and especially the ageing levels were involved into the proposed model by accurately addressing the model parameter values with higher resolution. The set-up of the comprehensive look-up tables for OCV-SOC relations, model parameters, and energy terms with respect to almost all the operational factors of the battery guaranteed the superior performance of the proposed model for online SOE and voltage prediction of the Li-ion battery.

VII. Conclusion

Different from the SOC, SOE represents the direct description of the residual available energy state of the battery, which is pivotal for the energy management and optimization in the smart grid applications. To predict the SOE, runtime, and the terminal voltage of the battery accurately, the battery behaviors under varying loads considering temperature and ageing effects are systematically analyzed and a comprehensive battery model is built accordingly. In specific, the key contributions of this work are summarized as: (1) a novel method to extract the parameters of the electrical model is proposed and it is capable of identifying the parameters with outperformed fidelity and acceptable computational burden; (2) the effects of the initial SOC, load current rate/direction, ambient temperature and the ageing level on the discharging performance of Li-ion batteries are investigated systematically and involved into the proposed model; and (3) test results on commercial Li-ion batteries validated the robustness and effectiveness of the proposed battery model against varying load, temperature and battery ageing influences, comparing to that most models in the literature were only verified on fresh cells under moderate loads and from fully charged states. The experimental results validated the efficacy of the proposed model with voltage prediction error less than 2%, SOE error no more than 4.7%, and runtime error within 1% under dynamic load conditions at an arbitrary ageing level. Last but not least, the proposed model is based on Matlab/Simulink and computationally light, thus it has the potential to be implemented in the BMSs of the ESSs in the smart grids applications. Following our previous studies on the online SOC and SOH co-evaluation of Li-ion batteries, this work provides a holistic understanding on the discharging behavior, terminal voltage and online SOE variation of Li-ion batteries exploited as ESSs in smart grids.

Future work will focus on the investigation of the irreversible and reversible energy loss of Li-ion batteries due to load variations, and the development of the energy loss and recovery rate of the battery with the consideration on idle time.

References

[1] B. Dunn, H. Kamath, and J.M. Tarascon, "Electrical energy storage for the grid: A battery of choices," *Science*, vol. 334, pp. 928-935, 2011.

[2] S. Vazquez, S.M. Lukic, E. Galvan, L.G. Franquelo, J.M. Carrasco, "Energy Storage Systems for Transport and Grid Applications," *IEEE Trans. on Ind. Electron.* vol. 57, no.12, pp. 3881-3895, 2010.

[3] DOE/EPRI 2013 Electricity Storage Handbook in Collaboration with NRECA, Tech. Rep. SAND 2013-5131, Sandia National Laboratories.

[4] X. Liu, J. Wu, C. Zhang, Z. Chen, "A method for state of energy estimation of lithium-ion batteries at dynamic currents and temperatures," *J. Power Sources* 270 (2014) 151-157.

[5] K. S. Ng, C. S. Moo, Y. P. Chen, and Y. C. Hsieh, "Enhanced coulomb counting method for estimating state-of-charge and state-of-health of lithium-ion batteries," *Appl. Energy*, vol. 86, no. 9, pp. 1506-1511, 2009.

[6] S. Lee, J. Kim, J. Lee, and B. H. Cho, "State-of-charge and capacity estimation of lithium-ion battery using a new open-circuit voltage versus state-of-charge," *J. Power Sources*, vol. 185, no. 2, pp. 1367-1373, Dec. 2008.

[7] H. He, R. Xiong, J. Peng, "Real-time estimation of battery state-of-charge with unscented Kalman filter and RTOS lCOS-II platform," *Appl. Energy* 2016, vol. 162, 1410-1418.

[8] I. Kim, "The novel state of charge estimation method for lithium battery using sliding mode observer." *J. Power Sources* 2006; 163: 584-90.

[9] J. Xu, C.C. Mi, B. Cao, J. Deng, Z. Chen, S. Li, "The state of charge estimation of lithium-ion batteries based on a proportional-integral observer," *IEEE Trans. on Veh. Technol.* 2014; 63:1614-1621.

[10] M. Charkhgard, M. Farrokhi, "State-of-Charge Estimation for Lithium-Ion Batteries Using Neural Networks and EKF," *IEEE Trans. Ind. Electron.*, 57 (2010), pp. 4178-4187.

[11] P. Singh, C. Fennie Jr., D. Reisner, "Fuzzy logic modelling of state-of-charge and available capacity of nickel/metal hydride batteries," *J. Power Sources*, 136 (2004), pp. 322-333.

[12] K. Mamadou, A. Delaille, E. Lemaire-Potteau, Y. Bultel, "The state-of-energy: a new criterion for the energetic performances evaluation of electrochemical storage devices." *ECS Trans.* 2010; 25:105-12.

[13] K. Mamadou, E. Lemaire, A. Delaille, D. Riu, S.E. Hing, Y. Bultel, "Definition of a state-of-energy indicator (SoE) for electrochemical storage devices: application for energetic availability forecasting." *J. Electrochem. Soc.* 2012; 159: A1298-307.

[14] G. Dong, X. Zhang, C. Zhang, Z. Chen, "A method for state of energy estimation of lithium-ion batteries based on neural network model." *Energy* 2015; 90:879-888.

[15] Y. Wang, C. Zhang, Z. Chen, "A method for joint estimation of state-of-charge and available energy of LiFePO4 batteries," *Appl. Energy* 2014; 135:81-87.

[16] Y. Wang, Z. Chen, C. Zhang, "On-line remaining energy prediction: A case study in embedded battery management system." *Appl. Energy* (2016), http://dx.doi.org/10.1016/j.apenergy.2016.05.081.

[17] L. Zheng, J. Zhu, G. Wang, T. He, Y. Wei, "Novel methods for estimating lithium-ion battery state of energy and maximum available energy." *Appl. Energy* 2016; 178:1-8.

[18] H. He, Y. Zhang, R. Xiong, C. Wang, "A novel Gaussian model based battery state estimation approach: state-of-energy," *Appl. Energy* 2015; 151:41-48.

[19] W. Zhang, W. Shi, Z. Ma, "Adaptive unscented Kalman filter based state of energy and power capability estimation approach for lithium-ion battery." *J. Power Sources* 2015; 289:50-62.

[20] H. Liu, H. Wang, C. Guo, "State of Energy Estimation Based on AUKF for Lithium Battery Used on Pure Electric Vehicle", *Advanced Materials Research*, Vols. 608-609, pp. 1627-1630, 2013.

[21] G. Dong, Z. Chen, J. Wei, C. Zhang, P. Wang, "An online model-based method for state of energy estimation of lithium-ion batteries using dual filters," *J. Power Sources* 2016; 301:277-286.

[22] C. Lin, H, Mu, R. Xiong, J. Cao, "Multi-model probabilities based state fusion estimation method of lithium-ion battery for electric vehicles: State-of-energy," *Appl. Energy* (2016), http://dx.doi.org/10.1016/j.apenergy.2016.05.065.

[23] F. Wei, S.C. Chien, Y.S. Hnin, K.J. Tseng, C.J. Spanos, S.K. Panda, "Condition monitoring system of Ubin Island micro-grid," in *Proc.2nd IEEE SPEC*, 2016; 1-6.

[24] F. Leng, C.M. Tan, R. Yazami, M.D. Le, "A practical framework of electrical based online state-of-charge estimation of lithium ion batteries," *J. Power Sources*, 255 (2014), pp. 423–430.

[25] A. Seaman, T.-S. Dao, J. McPhee, "A survey of mathematics-based equivalent-circuit and electrochemical battery models for hybrid and electric vehicle simulation", *J. Power Sources*, 256 (2014), pp. 410-423.
[26] M. Chen, G.A. Rincon-Mora, "Accurate electrical battery model capable of predicting runtime and I-V performance," *IEEE Trans. Energy Convers.*, 21 (2006), pp. 504-511.
[27] S. Abu-Sharkh, D. Doerffel, "Rapid test and non-linear model characterization of solid-state lithium-ion batteries," *J. Power Sources* 130 (2004) 266-274.
[28] A. Hentunen, T. Lehmuspelto, and J. Suomela, "Time-Domain Parameter Extraction Method for Thevenin-Equivalent Circuit Battery Models," *IEEE Trans. Energy Convers.* 2014, vol. 29, no. 3, pp. 558-566.
[29] L. Lam, P. Bauer, and E. Kelder, "A practical circuit-based model for Li-ion battery cells in electric vehicle applications," in *Proc. 33rd IEEE INTELEC*, 2011, pp. 1-9.
[30] T. Kim, W. Qiao, "A hybrid battery model capable of capturing dynamic circuit characteristics and nonlinear capacity effects," *IEEE Trans. Energy Convers.*, vol. 26, no. 4, pp. 1172-1180, Dec. 2011.
[31] S. Liu, J. Jiang, W. Shi, Z. Ma, L.Y. Wang, H. Guo "Butler-Volmer-equation-based electrical model for high-power lithium titanate batteries used in electric vehicles," *IEEE Trans. on Ind. Electron.* vol. 62, no.12, pp. 7557-7568, 2015.
[32] J. Jiang, S. Liu, Z. Ma, L.Y. Wang, K. Wu, "Butler-Volmer equation-based model and its implementation on state of power prediction of high-power lithium titanate batteries considering temperature effects," *Energy*, vol. 117, pp. 58-72, 2016.
[33] K. Li, B.H. Soong, K.J. Tseng, "A high-fidelity hybrid lithium-ion battery model for SOE and runtime prediction," in *Proc. IEEE APEC*, 2017, pp. 2374-2381.
[34] K. Li, K.J. Tseng, "Energy efficiency of lithium-ion battery used as energy storage devices in micro-grid," in *Proc. 41st IEEE IECON*, 2015; 5235-5240.
[35] K. Li, K. J. Tseng, L. Moraleja, "Study of the influencing factors on the discharging performance of lithium-ion batteries and its index of state-of-energy," in *Proc. 42nd IEEE IECON*, 2016; 2117-2123.
[36] X. Han, M. Ouyang, L. Lu, J. Li, Y. Zhang, Z. Li, "A comparative study of commercial lithium ion battery cycle life in electrical vehicle: aging mechanism identification," *J. Power Sources* 251 (2014), pp. 38-54.
[37] P. Svens, R. Eriksson, J. Hansson, M. Behm, T. Gustafsson, G. Lindberg, "Analysis of aging of commercial composite metal oxide - $Li_4Ti_5O_{12}$ battery cells," *J. Power Sources*, 270 (2014), pp. 131-141.
[38] R. Castaing, Y. Reynier, N. Dupré, D. Schleich, S. Jouanneau Si Larbi, D. Guyomard, P. Moreau, "Degradation diagnosis of aged $Li_4Ti_5O_{12}$/$LiFePO_4$ batteries," *J. Power Sources*, 267 (2014), pp. 744-752.
[39] T. Huria, M. Ceraolo, J. Gazzarri, R. Jackey, "High fidelity electrical model with thermal dependence for characterization and simulation of high power lithium battery cells," In *Proc. 2012 IEEE IEVC*, 2012; pp. 1-8.

Kaiyuan Li received the B.Eng. (First Class Honors) degree from Nanyang Technological University, Singapore, in 2014, where he is currently pursuing the Ph.D. degree from the School of Electrical and Electronic Engineering.

He is currently a Graduate Student Researcher with the Berkeley Education Alliance for Research in Singapore Limited, Singapore. His current research interests include intelligent battery management system design, modeling of Li-ion batteries, state estimation and energy efficiency of batteries, fast charging of Li-ion batteries, large-scale energy storage systems, and renewable energy generation and distribution in smart grids.

Feng Wei (S'10 M'14) is a research fellow with Singapore-Berkeley Building Efficiency and Sustainability in the Tropics. He received the B.Eng. degree from Wuhan University, in 2008 and Ph.D. degree from Nanyang Technological University, Singapore in 2014, both in Electrical Engineering. His research interests include doubly-fed induction generator, power quality, micro-grid monitoring and intelligent battery management system.

King Jet Tseng (S'85–M'88–SM'98) received the B.Eng. (first class) and M.Eng. degrees from the National University of Singapore, Singapore, and the Ph.D. degree in electrical power engineering from Cambridge University, Cambridge, U.K.

He was appointed as the Head of the Power Engineering Division, Nanyang Technological University (NTU), Singapore, for the maximum term of six years. He has been a Board Member of the Singapore Green Building Council, of the Advisory Board of the BCA Centre for Sustainable Buildings, and the Energy Standards Committee of Spring Singapore. He has been a Program Coleader of the Singapore-Berkeley Building Efficiency and Sustainability for the Tropics at Singapore's NRF-CREATE, and the Founding Director of the Electrical Power Systems Integration Laboratory, NTU, a Rolls-Royce research facility. He is currently a Professor and the Director of Electrical Power Engineering, Singapore Institute of Technology, Singapore.

Prof. Tseng is a Fellow of the Institution of Engineering and Technology (IET), U.K., the Institution of Engineers Singapore, and the Cambridge Philosophical Society, as well as a Chartered Engineer in the U.K. He has held a number of major appointments in professional societies including the Chair of the IEEE Singapore Section in 2005. He received the Swan Premium from the IET, the IEEE Third Millennium Medal, and the IEEE Region Ten Outstanding Volunteer Award.

Boon-Hee Soong (M'90–SM'04) received the B.Eng (Hons.) degree in electrical and electronic engineering from the University of Auckland, Auckland, New Zealand, in 1984, and the Ph.D. degree from the University of Newcastle, NSW, Australia, in 1990.

He is currently an Associate Professor with the School of Electrical and Electronic Engineering, Nanyang Technological University, Singapore. From October 1999 to April 2000, he was a Visiting Research Fellow with the Department of Electrical and Electronic Engineering, Imperial College, London, U.K., under the Commonwealth Fellowship Award. He has supervised many postgraduate students and postdoctoral researchers in the area of optimization of mobile and wireless communication networks. He has published extensively in international journals and conferences papers, monographs, textbooks, and several relevant patents.

Dr. Soong is a member of ACM. He received the Tan Chin Tuan Fellowship in 2004 and visited Duke University, Durham, NC, USA.